Measurement 235 (2024) 114905

Contents lists available at ScienceDirect

Measurement

journal homepage: www.elsevier.com/locate/measurement

A novel method for holdup measurement of three phases by an ultrasonic device with the flexible substrate

Jinhui Fan [a], Hang Liu [b], Haibin Cui [a], Wenyuan Wang [a], Jizhou Song [b,c,*], Fei Wang [a,*]

[a] State Key Laboratory of Clean Energy Utilization (Zhejiang University), Hangzhou, China, 310027
[b] Department of Engineering Mechanics, Soft Matter Research Center, and Key Laboratory of Soft Machines and Smart Devices of Zhejiang Province, State Key Laboratory of Brain-Machine Intelligence, Zhejiang University, Hangzhou 310027, China
[c] Department of Rehabilitation Medicine, The First Affiliated Hospital, School of Medicine, Zhejiang University, Hangzhou 310003, China

ARTICLE INFO

Keywords:
Phase holdup
Flexible substrate
Ultrasonic reflection
Transit-time

ABSTRACT

The precise measurement of multiphase flow holds significant importance across diverse industrial contexts. However, rigid probes struggle with the variable dimensions of curved surfaces, while flexible probes are hindered by fragility, susceptibility, and challenges in large-scale production. Herein, we propose an ultrasonic device featuring a flexible substrate that seamlessly amalgamates flexibility and rigidity to enable precise measurement of three-phase flow. Through simulation, we determine the optimal ultrasonic frequency (1 MHz) and flexible substrate thickness (3 mm) for a specified probe and pipe size (20 mm). A novel concept, the specific attenuation coefficient (SAC), derived from the voltage-amplitude of transmitted and received signals and propagation distance, is introduced to differentiate between oil and water. The discrepancy between measured and actual three-phase holdups are 0.55 %, 0.36 %, and 0.59 % for water, gas and oil, respectively, with a variance of measurement results 0.027.

1. Introduction

The mixed transport of oil, gas, and water characterizes a common multiphase flow scenario in the petrochemical industry [1–3]. Accurate characterization of phase holdup in water–gas-oil multiphase flow is crucial for investigating flow mechanisms, exploring the properties of underground crude oil, and achieving the safe and efficient extraction [4–7]. Unlike the simple single-phase fluids, multiphase flow encounters the challenges of response nonlinearity and spatiotemporal non-uniform distribution at the interphase interface, which makes it difficult to distinguish phases accurately, particularly in high speed, remote control, and non-invasive measurement occasions [8,9]. Considerable methods have been applied to solve above mentioned challenges, such as electrical, optical, and tomography techniques. However, each of them holds distinct merits and shortages tailored to specific applications. For instance, the electrical method offers a low cost and rapid response but is constrained by the requirement for specific electrical properties in the measurement object. Optical techniques exhibit elevated measurement precision and short response time, their applicability yet is confined to materials characterized by favorable light transmission properties, rendering them ineffectual for materials impervious to light penetration. Tomography is equipped with high resolution and high sensitivity, and can also provide detailed internal structure information, however, it requires multiple sensors to be arranged around the pipeline to be measured, posing challenges for widespread use in complex industrial settings [10–13].

One another practical technique for monitoring multiphase flow is the acoustic method. As a non-invasive procedure, ultrasound boasts robust penetration and directivity, enabling its application in dense suspensions and optically opaque liquids. Its cost-effectiveness, rapid response, and user-friendly nature render it particularly suitable for the demanding operational conditions prevalent in the petroleum industry [10,15]. The foundational principle of ultrasonic measurement hinges on sound waves encountering transmission, reflection, scattering, interference, and other phenomena within the flow field, leading to variations in ultrasonic characteristic coefficients. These coefficients, encompassing frequency, amplitude, and phase of transmitted and received signals, offer valuable insights into the flow condition of multiphase fluid [16,17].

The majority of existing studies on ultrasonic multiphase flow have primarily focused on advancing data analysis methods to achieve greater accuracy in measuring parameters such as flow pattern,

* Corresponding authors.
E-mail addresses: jzsong@zju.edu.cn (J. Song), wangfei@zju.edu.cn (F. Wang).

https://doi.org/10.1016/j.measurement.2024.114905
Received 17 January 2024; Received in revised form 6 May 2024; Accepted 12 May 2024
Available online 19 May 2024

ultrasonic [18–19]. However, there remains a notable gap in research concerning measurement devices. Typically, commercial devices for evaluating multiphase flow exhibit rigid structures incapable of significant deformation. The fixed-size transducers depicted in Fig. 1a significantly limit their adaptability, particularly in small-diameter pipes where their utility is diminished and the introduction of air gaps inevitably leads to amplitude errors and inaccurate results. Consequently, recent attention has been directed toward flexible ultrasonic sensors due to their inherent versatility and lightweight properties [21], positioning them as promising candidates [22,23]. Fig. 1b demonstrates limitations of rigid probe applications and the adaptability of flexible devices in specialized measurement scenarios, thus significantly expanding the potential for sensor applications across various domains, including communication, energy, medicine, and national security [21,24]. However, it is imperative to acknowledge that while flexibility enhances adaptability to complex pipe curvatures and industrial environments, its intrinsic fragility may lead to relatively short working lifespans. As depicted in Fig. 1b, the flexible core of the device, represented by the serpentine wires, guarantees the favorable ductility but exacerbates their fragility due to the micron-level cross-sectional size. Moreover, the intricate and costly production processes involving lithography, etching, and coating equipment, coupled with susceptibility to damage at each step, pose substantial challenges to mass production, severely limiting the industrial applications of flexible devices [25–26]. Therefore, efficiently amalgamating the durability inherent in rigid probes within the industrial domain and the versatile adaptability of flexible probes to various curved pipes stands as a pivotal focus, promising to significantly enhance adaptability, accuracy, and cost-effectiveness in pipeline-fluid measurement.

In this work, an innovative approach is presented for measuring the holdup of three phases in small-size pipelines using an ultrasonic device with the flexible substrate. Different flexible substrates and ultrasonic frequencies will yield varying effects on the measurement results. In order to select a suitable flexible base, the COMSOL software was utilized to investigate the influence of the thickness and ultrasonic frequency of the flexible substrate on the measurement results. The device, consisting of two identical components, features a flexible substrate as its key element, ensuring compatibility with pipes of various sizes for precise measurements through the incorporation of rigid probes. This advancement allows the rigid probe to effectively conform to diverse surfaces, achieving a balance between the adaptability of the flexible probe and the durability of the rigid probe. This effort, which focuses on optimizing the measurement equipment and thus improving the measurement results, is neglected by existing three-phase flow studies, As such, it is considered to be the first central highlight of this paper. In addition, the paper delves into the analysis of phase holdup measurement, commencing with the determination of transit-time after ultrasonic reflection at the gas–liquid interface, unveiling the liquid and

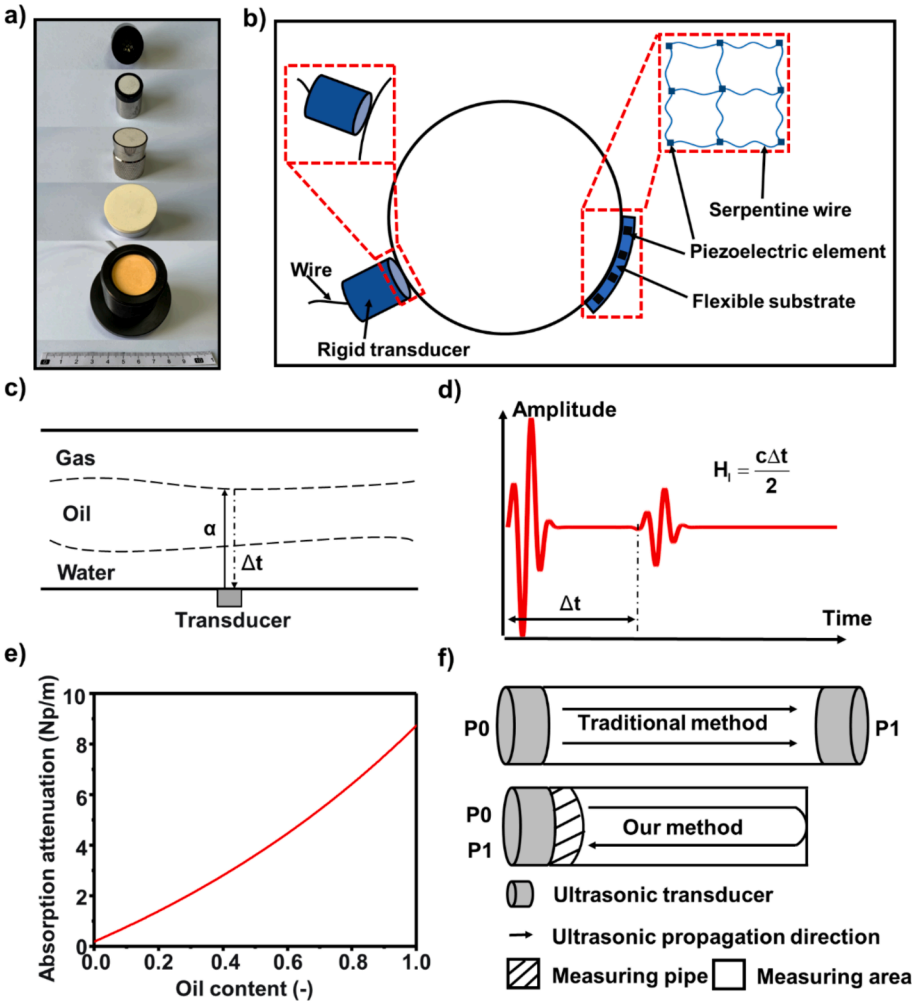

Fig. 1. (a) Rigid probes with fixed sizes commonly utilized in industry. (b) Adaptability comparison between rigid and flexible devices: limitations of rigid probe applications and the core of the flexible devices: stretchable wires. (c) Schematic diagram of ultrasonic reflectance at oil–gas interface. (d) Diagram of height acquisition of the liquid phase based on ultrasonic reflectance. (e) Relationship between absorption attenuation and oil content. (f) The difference of ultrasonic transmission path between traditional method and our method.

subsequently the gas height. Additionally, a new concept of Specific Attenuation Coefficient (SAC) is introduced to characterize the water and oil phases, which stems from the linear relationship between SAC and oil phase content in the liquid phase. Specific Attenuation Coefficient can be obtained based on the voltage-amplitude of the transmitted and received signal and the propagation distance. As a concept initially proposed, it is regarded as the second core highlight of this paper. We set up a multiphase flow experimental platform and utilized the flexible wearable device to characterize the phase holdup. Ultimately, the error in the measured holdup for all three phases was less than 1 %, demonstrating the accuracy of the measurement method. In the realm of industrial multiphase flow measurement, this method offers the advantages of simplicity in operation, strong adaptability, accurate results, and low-cost, facilitating the precise determination of three-phase holdup in oil–gas-water flow scenarios.

2. Methodology

2.1. Gas phase holdup determination by ultrasonic transit-time

In the context of three-phase flows, phase holdup serves as a parameter describing the proportion of each phase component to the total component, which can be categorized into section phase holdup, volume phase holdup, and mass phase holdup. The section phase holdup refers to the ratio of the section area of each phase to the total area on the pipeline section [18]. In this work, however, the height occupied by the three phases in the pipeline is considered as the assessment criterion of the section phase holdup to simplify the calculation.

Acoustic impedance, expressed as the product of sound speed and density, is a key factor [28], with water, oil, and gas having acoustic impedances of $1.50\times\ 10^6$ Pa·s/m^2,$0.98\times\ 10^6$ Pa·s/m^2, and 445.9 Pa·s/m^2, respectively. The acoustic impedance of two phases is crucial for determining sound pressure reflectance and transmittance when ultrasonic waves traverse water–oil and oil–gas interfaces, described as follows [29]:

$$R_{(w/o)}=\frac{\rho_o c_o-\rho_w c_w}{\rho_o c_o+\rho_w c_w}=-20.97\% \tag{1}$$

$$T_{(w/o)}=\frac{2\rho_o c_o}{\rho_o c_o+\rho_w c_w}=79.03\% \tag{2}$$

$$R_{(o/g)}=\frac{\rho_g c_g-\rho_o c_o}{\rho_g c_g+\rho_o c_o}=-99.91\% \tag{3}$$

$$T_{(o/g)}=\frac{2\rho_g c_g}{\rho_g c_g+\rho_o c_o}=-0.09\% \tag{4}$$

where, R and T denote reflectance and transmittance, respectively; w, o, and g is water, oil, and gas, respectively; w/o and o/g refer to the interfaces of water–oil and oil–gas, respectively.

The formulations indicate that a predominant portion of the ultrasonic wave traverses the oil and enters the water, exhibiting a 20 % reflectance at the water–oil interface. Yet, due to the considerable difference in acoustic impedance between the gas and liquid at the gas–liquid interface, up to 99.91 % of the ultrasonic energy is reflected by the interface. Hence, upon traveling through the liquid phase, the ultrasound will be reflected at the liquid–gas boundary (depicted in Fig. 1c), and the received reflected signals signify the height of the liquid phase. Comparing the time-domain difference between the transmitted signal and the reflected echo signal, the height of the liquid phase can be obtained after multiplying the time difference by the speed of sound, as illustrated in Fig. 1d. The height of the liquid phase can then be subtracted from the pipe's diameter to ascertain the height of the gas phase.

2.2. Ultrasonic attenuation in a liquid phase

Ultrasonic attenuation denotes the process wherein sound strength diminishes with increasing distance as it travels through a liquid phase. The energy losses revealed by ultrasonic attenuation are primarily attributed to beam diffusion (dependent on transducer structure) and absorption (related to thermos-elastic and viscoelastic effects) [30,31]. In this work, the experimental distance is confined to a small range (within 40 mm), thus the diffusion losses can be disregarded and absorption is solely taken into account. The attenuation coefficient, indicating the loss in sound intensity per unit length of the propagation path, is defined as follows [31,32]:

$$\alpha=-\frac{\ln\frac{P}{P_0}}{L} \tag{5}$$

where, P and P_0 are the sound pressure and the original sound pressure, α denotes the attenuation coefficient, L is the ultrasonic propagation distance.

The absorption attenuation coefficient in oil–water two-phase flow, as proposed by Su et al., is expressed as [33]:

$$\alpha_{abs}=\frac{8\pi^2 f^2\eta}{3[\rho_1(1-\varphi_V)+\rho_2\varphi_V]c^3} \tag{6}$$

where, f is the frequency of sound wave; η is the viscosity in the liquid; ρ_1 and ρ_2 represent the density of water and oil, respectively; φ_V is the oil phase holdup; c is the sound velocity in the medium. The ultrasonic absorption attenuation variations with phase holdup are illustrated in Fig. 1e, as a result of substituting the physical characteristics of oil and water from Table 1 into the absorption attenuation model. It can be seen that the absorption attenuation increases with oil content, benefiting from its viscosity is greater than that of water. Therefore, the absorption attenuation coefficient raises gradually with the oil phase holdup, while the viscosity plays a dominated role in this process.

2.3. Specific attenuation coefficient (SAC)

As shown in the Fig. 1f, in general, ultrasound is received after transmission through the measurement area. However, in our experiment, ultrasound follows a distinct path—entering the measurement pipeline after transmission, progressing through the measurement area, reaching the gas–liquid interface at a certain distance, reflecting back, and eventually being received after traversing the measurement area and pipeline again. This paper centers on the analysis of signals captured by the ultrasonic device, particularly ultrasound reflected upon encountering the reflection interface following traversal through the liquid phase. Consequently, the observed attenuation is influenced by both the reflection interface and the characteristics of the liquid phase. Thus, to avoid ambiguity with the universal attenuation coefficient, the Specific Attenuation Coefficient (SAC) is introduced herein. SAC can be determined based on the voltage-amplitude of the transmitted and received signals as well as the propagation distance.

Table 1
Physical parameters of oil, water and nitrogen (25 °C).

Physical parameters	Sound velocity (m/s)	Density (kg/m^3)	Viscosity (mPa·s)	Thermal conductivity (W/m/K)	Specific heat capacity (J/kg/K)
Water	1497	998	1.0087	0.6	4179
Oil	1421	760	57.1	0.2	2000
Nitrogen	348.6	1.257	0.0178	0.025	1038

3. Experiments

3.1. Fabrication of the ultrasonic device with the flexible substrate

3.1.1. Simulation

The precision of measurements exhibits variability across different pipe sizes, prompting the necessity to identify the most appropriate ultrasonic frequency and flexible substrate thickness for each scenario. To address this, we employed COMSOL simulation software to evaluate the accuracy of ultrasonic measurements across three distinct pipe diameters while maintaining a consistent probe size. The simulations entailed an exploration of the impact of ultrasonic frequency and flexible substrate thickness on the results [34,35]. The findings are illustrated in Fig. 2, providing a comprehensive analysis of ultrasonic propagation across various frequencies and flexible substrate thicknesses, each corresponding to different combinations of probe and pipeline sizes.

Upon comparison of Fig. 2a, 2c, and 2e, optimal sound field conditions are observed when the probe size matches the pipe size (20 mm). Combining Fig. 2a and 2b leads to the conclusion that, for this specific probe-to-pipe size ratio, the optimal ultrasonic frequency and flexible substrate thickness are 1 MHz and 1 mm, respectively, yielding the highest measurement efficacy. Similarly, incorporating Fig. 2c and 2d indicates that an ultrasonic frequency of 2 MHz and a flexible substrate thickness of 1 mm result in the most accurate measurements. Furthermore, a comprehensive evaluation of Fig. 2e and 2f indicates that the ultrasonic frequency and flexible substrate thickness should be determined as 1 MHz and 3 mm, respectively. Therefore, after thorough analysis, we have determined that for the experimental setup, a probe and pipe size of 20 mm, an ultrasonic frequency of 1 MHz, and a flexible substrate thickness of 3 mm offer the most effective configuration.

For the same transducer, higher ultrasonic frequencies enhance the directivity of the ultrasonic beam and concentrate energy more effectively. However, concurrently, with increased ultrasonic frequency, attenuation accelerates in the propagation process. Therefore, selection of the most appropriate frequency should involve comprehensive considerations.

Regarding the thickness of the flexible substrate, due to the substantial acoustic impedance disparity between the piezoelectric material and the medium to be measured, strong reflection occurs as sound waves traverse the interface directly. It becomes necessary to introduce a matching layer (or layers) between them to achieve impedance matching and reduce reflection. Consequently, the flexible substrate functions as a matching layer, with its thickness and parameters are determined by acoustic characteristics. For the working environment and parameters in the simulation, the matching layer of 3 mm is deemed optimal.

For a detailed description of the simulation procedure, Supplementary Information 1 is provided [21].

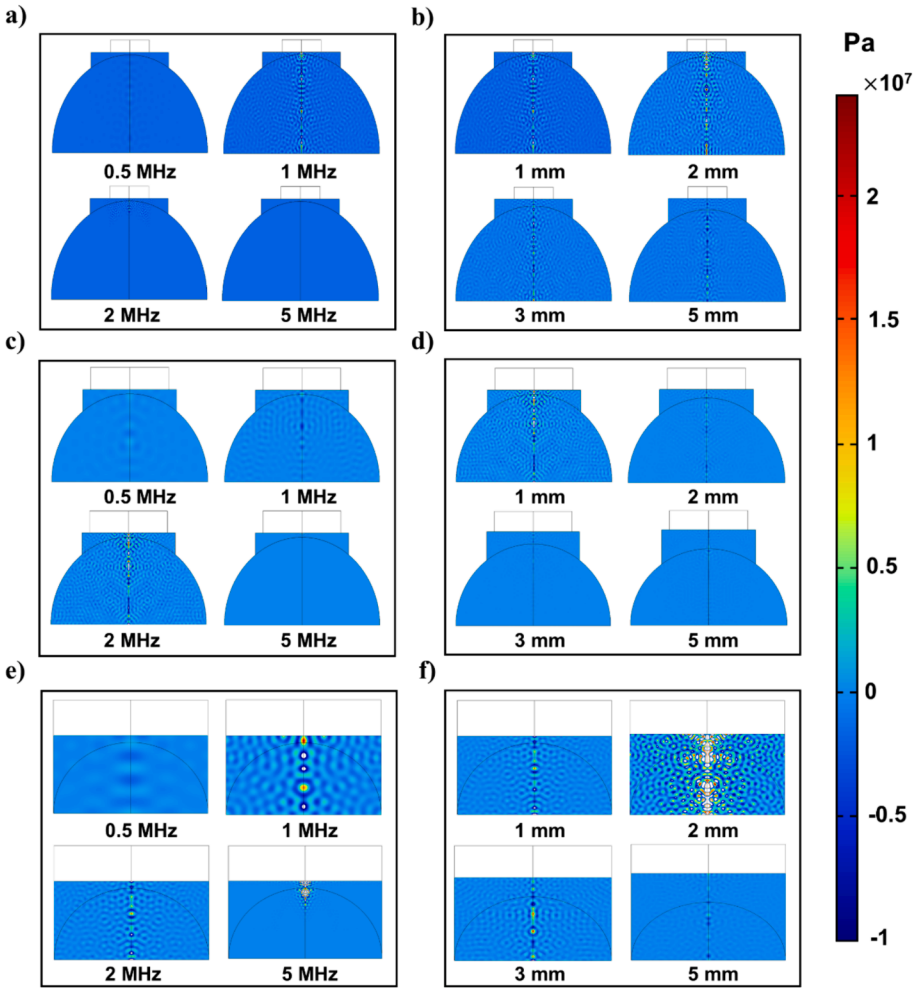

Fig. 2. Total sound pressure field with various ultrasonic frequency and flexible substrate thickness. (a) Total sound pressure field at different frequencies when the probe is 20 mm and the pipeline is 80 mm. (b) Total sound pressure field under varying flexible substrate thicknesses for a 20 mm probe and an 80 mm pipe. (c) Total sound pressure field at different frequencies when the probe is 20 mm and the pipeline is 40 mm. (d) Total sound pressure field under different flexible substrate thicknesses for a 20 mm probe and a 40 mm pipe. (e) Total sound pressure field at different frequencies when the probe is 20 mm and the pipeline is 20 mm. (f) Total sound pressure field under different flexible substrate thicknesses for a 20 mm probe and a 20 mm pipe.

3.1.2. Determination of flexible substrate components

In the experiment, Polydimethylsiloxane (PDMS) and curing agent were blended in various proportions to create a suitable probe 'jacket'. PDMS, a polymer silicone compound known for its optical transparency, inertness, non-toxicity, and non-flammability, stands as a commonly used silicon-based organic polymer material, extensively applied in biology, hospitals, and diverse fields [36,37]. When combined with the curing agent, also known as a hardener or setting agent, they generate a transparent, deformable, and cost-effective elastomer, easily adhering to objects [38].

Five flexible substrates were crafted with PDMS to curing agent ratios of 10:1, 20:1, 30:1, 40:1, and 50:1. After mixing evenly, the compounds underwent vacuum drying in a DZF-6050 model oven in 1 h to eliminate bubbles, followed by curing at 60 °C for 4 h in a GZX-9030MBE electric blast drying oven [39,40]. Steel balls with the diameter of 3 cm were placed into each sample to assess their softness and adhesion, and the illustrations showcasing the results can be found in Figure S2. It is concluded that the softness and adhesion of flexible substrate increase with the percentage of PDMS, however, the adhesion of the mixture is too excessive when the ratio is 50:1, as evidenced by the

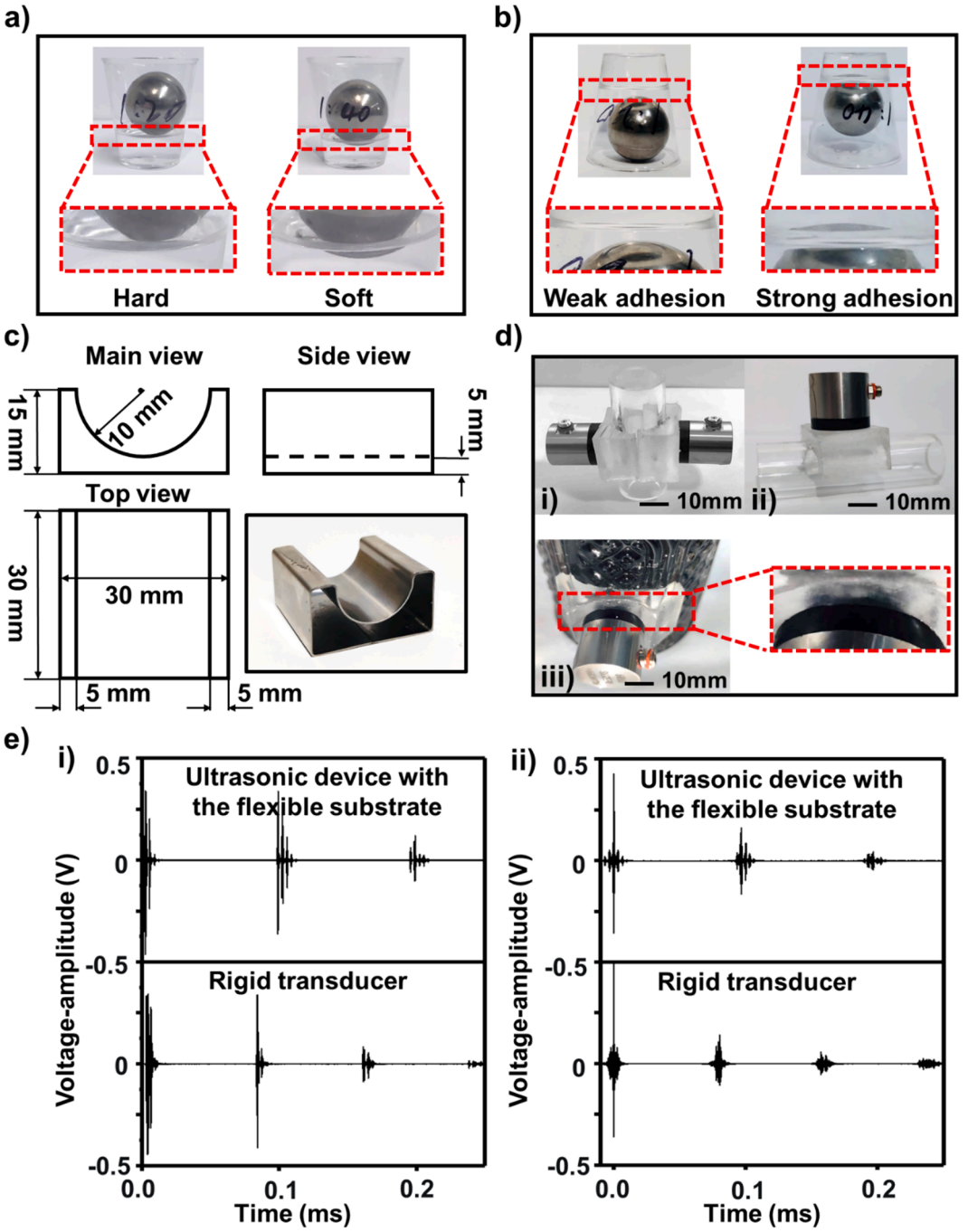

Fig. 3. (a) The softness of two samples with PDMS to curing agent ratios of 20:1 and 40:1. (a) The adhesion of two samples with PDMS to curing agent ratios of 20:1 and 40:1. (c) Three views of the flexible substrate mold and the final designed mold. (d) Applications of the ultrasonic device with flexible substrate in pipeline measurement: (i) the arrangement of the ultrasonic device with flexible substrate around the pipeline. (ii) the side view of the ultrasonic device with flexible substrate applied in the pipeline. (iii) the adaptability of the ultrasonic device with flexible substrate on uneven surfaces. (e) Comparison of measurement voltage-amplitude of the ultrasonic devices with flexible substrate and rigid devices under the same condition: (i) the original signal. (ii) the processed signal.

steel ball not falling after container inversion for 60 s. Fig. 3a and 3b exhibits the comparison of softness and adhesion that attributes to 20:1 and 40:1, respectively, and consequently, the ratio of 40:1 is applied for the manufacture of flexible substrate.

3.1.3. Fabrication of the ultrasonic device with the flexible substrate

The thickness of the flexible substrate determined through simulation is 3 mm, matching the diameter of the probe and the pipe at 20 mm. Consequently, a mold for the flexible substrate was crafted under these experimental parameters, and Fig. 3c presents three views and an actual image of the final designed mold. As mentioned above, PDMS and the curing agent, mixed at a ratio of 40:1, was selected to fabricate the flexible substrate. After that, the mold was treated with a RD-518 fluorin release agent to facilitate the subsequent removal. This flexible substrate, showcased in Fig. 3d, exhibits remarkable adaptability to pipes of varying sizes. In addition, the flexible substrate can also effectively cover some slightly convex interfaces, which is highly adaptable to the actual industrial situations. Fig. 3e presents a comparison of echoes obtained by the ultrasonic device with a flexible substrate and a rigid straight probe when measuring the same measured object. Given the emission of 12,500 pulses per second, the volume of collected data is substantial. To facilitate comparison in both the time domain and voltage-amplitude, only selected periods are displayed herein. The left segment depicts the time domain signals acquired by the two transducers, while the right segment illustrates the temporal information following autocorrelation processing. Discrepancies observed in the time domain signal indicate the thickness of the flexible substrate, and it is evident that the difference in voltage-amplitude is almost negligible, which confirms the precise measurement capabilities of the ultrasonic device with the flexible substrate.

3.2. Experimental process

The estimation of phase holdup in the three-phase flow is conducted utilizing an ultrasonic device equipped with a flexible substrate. The experimental setup comprises several components, including a gas flowmeter, two peristaltic pumps, a data acquisition card, a gas tank, two high-voltage pulse transmitter receivers, a converter circuit board, an experimental pipeline, an ultrasonic device with a flexible substrate, and three barrels, as depicted in Fig. 4a. Furthermore, Fig. 4b presents a detailed schematic of the ultrasonic device with the flexible substrate.

Oil and water are contained within respective barrels (identified as

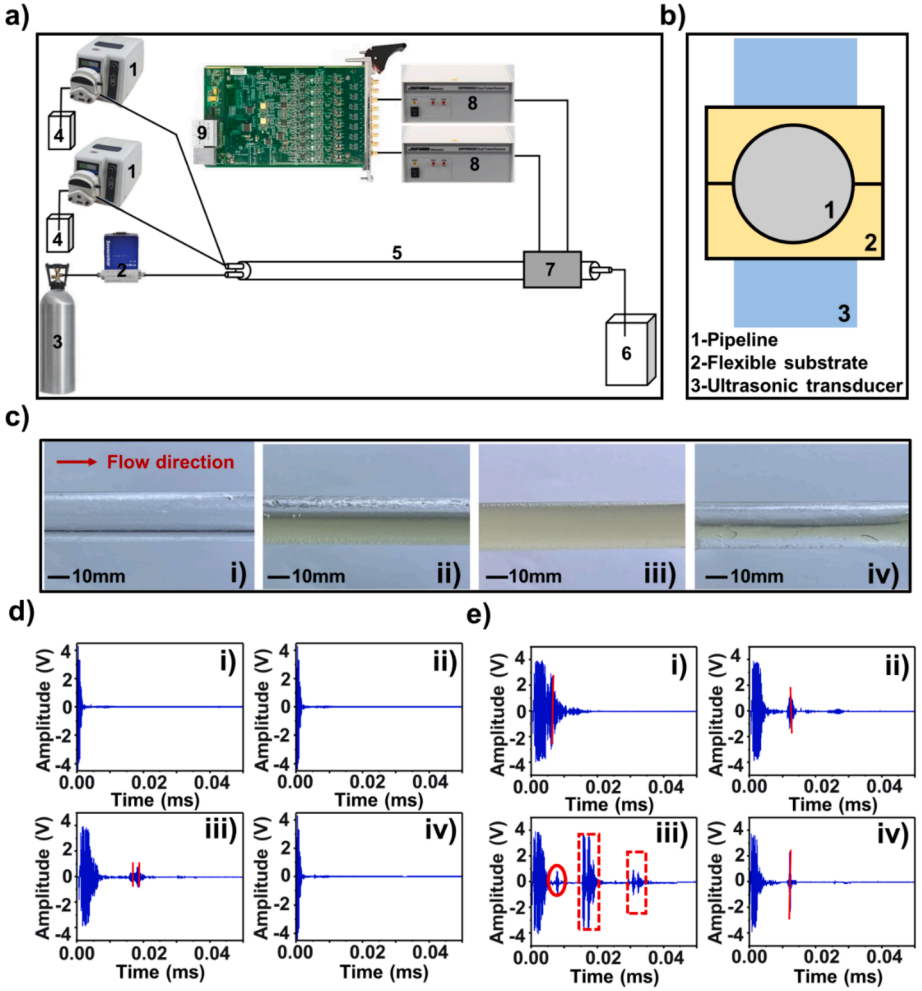

Fig. 4. (a) Experimental devices for monitoring phase holdup: 1-peristaltic pumps, 2-gas flowmeter, 3-gas tank, 4-barrels for oil and water, 5-experimental pipeline, 6-recycling barrel, 7-the ultrasonic device with the flexible substrate, 8-high-voltage pulse transmitter receivers, 9-data acquisition card. (b) Detailed diagram of the ultrasonic device with the flexible substrate. (c) Actual photographs of four multiphase flows: (i) water–gas two-phase flow. (ii) oil–gas two-phase flow. (iii) oil–water two-phase flow. (iv) water–oil–gas three-phase flow. (d) The received signals of probe up in four flows: (i) the received signals of probe up in water–gas two-phase flow. (ii) the received signals of probe up in oil–gas two-phase flow. (iii) the received signals of probe up in oil–water two-phase flow. (iv) the received signals of probe up in water–oil–gas three-phase flow. (e) The received signals of probe down in four flows: (i) the received signals of probe down in water–gas two-phase flow. (ii) the received signals of probe down in oil–gas two-phase flow. (iii) the received signals of probe down in oil–water two-phase flow. (iv) the received signals of probe down in water–oil–gas three-phase flow.

device No. 4 in Fig. 4a) prior to their subsequent pumping into the pipe. Each barrel measures 10 cm × 10 cm × 50 cm, equating to a volumetric capacity of 5 L for each liquid. The laboratory infrastructure is adequately provisioned with ample reserves of oil and water to facilitate prompt replenishment of these barrels. The peristaltic pump employed for the conveyance of oil and water originates from Kamoer Company, designated as model UIP WIFI-S243K-GB, and is complemented by #18 (7.9*11.1 mm) hose. Additionally, a gas cylinder (device No. 3 in Fig. 4a) boasting a capacity of 20 L is employed for gas storage. The transmission of gas is facilitated through the laboratory's gas conduits, employing transparent PVC hoses, and regulated by a gas flow meter (Seven Star, CS series, 50 mL/min). Throughout the experiment, manipulation of the relative flow rates among the three constituents affords direct control over the phase composition within the pipeline. The ultrasonic device with the flexible substrate can be perfectly wrapped around the exterior of the plexiglass pipe, allowing for phase holdup determination within the pipe using the two probes positioned vertically. The high-voltage pulse transmitting receiver (JSR Company, DPR300) allows for independent control over the pulse amplitude, energy, repetition rate, and high and low pass filters. The data acquisition card, attached to the high-voltage pulse transmitting receiver, facilitates signal sampling and data storage. The experiment utilizes the Art Technology PXIe 8584 data acquisition card, an 8-channel, 14-bit sampler with a sampling rate of 100 MS/s specifically designed for high-frequency frequencies exceeding 50 MHz. To adhere to the Nyquist sampling law, the experiment employs an ultrasonic frequency of 5 MHz and a sampling rate of 20 MS/s [41]. Following the measurement, the oil-and-water mixture is disposed of in the recycling bin to conclude the experimental procedure.

The experiments encompass four distinct scenarios: water–gas two-phase flow, oil–gas two-phase flow, oil–water two-phase flow, and water–oil–gas three-phase flow (as depicted in Fig. 4c). For oil–gas, water–gas and oil–water two-phase flow, the stratified flow is obtained mainly by controlling the flow rates of both phases while simultaneously observing real-time flow pattern information in the experimental pipe section. Typically, maintaining a fixed flow rate for one phase while altering the flow rates of the other two phases is necessary to induce three-phase stratified flow. In this specific experiment, the attainment of a consistent three-phase flow necessitates a sequential procedure. Initially, oil and water are pumped into the pipeline (the flow rate of one phase can be set as constant while varying the other to achieve a stable oil–water interface). Upon achieving a stable two-phase stratified flow, the flow rates of both constituents are held constant, while the introduction of gas is adjusted from minimal to maximal levels until a stable three-phase stratified flow is attained. Sustaining the constancy of flow rates for all three phases ensures the prolonged stability of the three-phase stratified flow, thereby facilitating the desired measurements over an extended duration. Ultimately, the flow rate of the fixed oil phase is set at 0.25 L/min, equivalent to 0.013 m/s (with a 20 mm diameter for the experimental pipe section). Subsequently, the flow rates of the water and gas phases are systematically adjusted until an undetermined three-phase flow is attained. The recorded flow rates for water and gas at this juncture are 0.36 L/min and 200 sccm, corresponding to flow velocities of 0.019 m/s and 0.011 m/s, respectively. At this stage, the ratio of the flow rates for the three phases (oil, gas, and water) is 25:20:36, aligning with the respective phase holdups of 30.87 %, 24.69 %, and 44.44 %. Two supplementary experiments were conducted to confirm that the corresponding three-phase stratified flow could be obtained through adjustments in the corresponding flow rates.

The Reynolds number is introduced to characterize the flow, representing the ratio of inertial and viscous forces[42]. A low Reynolds number implies that viscous force dominates the flow field over inertia, resulting in velocity disturbance attenuation by viscous force, thus yielding stable laminar flow. Specifically, in tubular flows, flows with Reynolds numbers less than 2300 are laminar characteristics [43,44]. Table 2 indicates that all four multiphase flows generated in the experiment are characterized by laminar flow conditions (the corresponding data are derived from Table 1). The evolution of the generated multiphase stratified flow is monitored over time, with the signals received by the upward and downward-oriented probes depicted in Fig. 4d and Fig. 4e, respectively.

Table 2
Relevant parameters for Reynolds number calculation.

Parameters	water–gas	oil–gas	oil–water	water–oil–gas
Density(ρ)/(kg/m^3)	151.07	736.25	928	728.71
Velocity(v)/(m/s)	0.0155	0.0800	0.0814	0.0317
Characteristic Length(d)/m	0.02	0.02	0.02	0.02
Viscosity coefficient(μ)/cp	1.0017	57.0805	51.0557	22.8651
Reynolds number	0.0467	0.0206	0.0296	0.0202

4. Results and analysis

Firstly, the analysis focuses on the four images in Fig. 4d (probe positioned upward at the top of the pipeline). Obviously, three of the figures in Fig. 4d show only transmission signals without any echo, indicating that the ultrasound was failed to penetrate the pipe, with reflection occurring on the pipe wall. This total reflection is attributed to the significant acoustic impedance difference between the gas phase and the plexiglass wall surface, signifying the presence of gas at the top of the pipeline. In the lower-left corner of Fig. 4d, the signals indicate ultrasound penetration into the pipeline with reflection, suggesting the absence of gas above the pipeline, implying the filling of the pipeline with the liquid phase. In fact, the echo around 0.02 ms is a result of the pipe wall reflection, and the two time-domain signals represent the thickness of the pipe. Notably, the reflected signals of the downward probe for the water–gas and oil–gas two phases exhibit essentially the similar contour, which implies that the ultrasound is reflected back at the gas–liquid interface after passing through the liquid phase. Signals of probe up indicated that ultrasound is directly transmitted back by the wall surface and caused some residual vibration. Both probes, up and down, for the oil–water phase traverse the entire pipe and are reflected off the opposite side of the wall, resulting in similar waveforms.

Fig. 4e shows the detection signals of the probe below in four cases. The time domain highlighted by the red line corresponds to the height of the liquid phase, and the circle in the data at the lower left corner indicates the division between the oil and water phases, and the red dashed line box indicates two cycles in which the ultrasound propagates twice. It should be noted that reflected signals may be picked up at the oil–water interface (the red circle in Fig. 4e) when the phase holdup of the oil–water two phases changes. However, since the reflected signals at the oil–water interface are not always obvious, it is more accurate to use the Specific Attenuation Coefficient (SAC) to reflect the oil phase holdup in the liquid phase in this manner. The features of the reflected signal for a three-phase flow may be interpreted as the unity of 'water–oil + oil-gas', allowing the gas phase content can be ascertained using time-domain data. Subsequently, the phase holdup of the oil and water two phases can be estimated through SAC.

Furthermore, we use COMSOL to simulate ultrasonic emission and reception in the presence of multiphase. Geometry and material parameters in simulation are shown in Fig. 5a, where phase 1 is gas, phase 2 is oil, and phase 3 is water due to density differences. Assuming that oil and water each account for 50 % of the liquid phase, the SAC under different liquid content is simulated, and the ratio of simulated SAC to SAC in the pipeline filled with liquid phase is calculated respectively [17,45,46], as shown in Fig. 5b. In addition, SAC is simulated with different percentages of oil phase in the liquid phase under five cases: 100 %, 80 %, 60 %, 40 %, and 20 % of the total liquid content. Fig. 5c displays the signal from the probe down when the pipeline is filled with pure water and pure oil, namely with oil contents of 0 % and 100 %, and the SACs under these two situations are 2.04 Np/m and 25.76 Np/m,

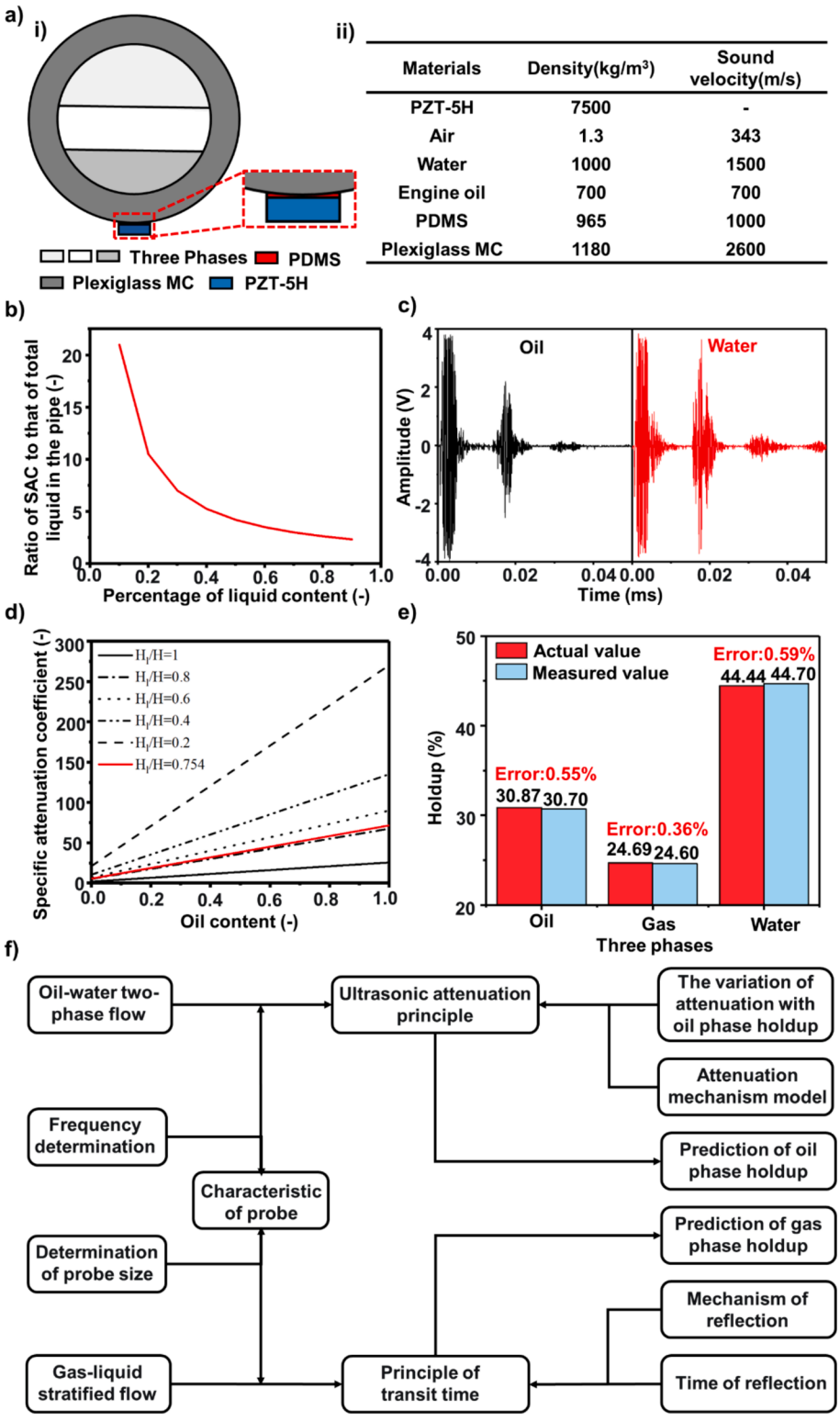

Fig. 5. (a) Geometry and material setup in simulation: (i) the geometry of the model. (ii) the parameter setting of the model. (b) Relationship between the SAC ratio and percentage of liquid content. (c) The signal from the probe down when the pipeline is filled with pure water and pure oil. (d) Variation of the SAC with oil content under different liquid contents. (e) Comparison of measurement and actual results of three phase holdups. (f) Step diagram for solving the holdups of the three phases.

respectively (according to Equation (5). Combining the simulation results and Fig. 5c, the variation of the SAC with oil content is established, serving as the basis for determining the oil phase holdup in subsequent experiments, as illustrated in Fig. 5d.

Subsequently, the data pertaining to the fourth case (oil–gas-water three-phase flow) are subjected to detailed analysis to delineate the process of determining each phase holdup. Initially, the signal in Fig. 4e (probe down below the pipeline) undergoes a detailed analysis, and the signal autocorrelation analysis (analytical process is recorded in Supplementary Information 3) manifests that the time corresponding to

signal reflection is 0.012 ms, and the height of liquid phase is 7.54 mm (the calculation process is elucidated in Fig. 1d), that is, the height of gas phase is 2.46 mm [47,48]. Considering the liquid phase constitutes 75.4 % (calculated as the ratio of liquid phase height, 7.54 mm, to pipe diameter, 10 mm), the corresponding relationship between SAC and oil phase holdup is established (illustrated by the red line in Fig. 5d). After that, the height of the oil and water phases within the liquid phase are distinguished as follows: Given the voltage-amplitude of original and the reflected signals are 4.59 V and 7.70 V, respectively, Equation (5) dictates that the corresponding SAC is 32.57 Np/m. By referencing the red line in Fig. 5d, the oil phase content is computed to be made up 40.7 % of the total liquid when the corresponding SAC equals 32.57 Np/m. This implies that the oil phase height accounts for 30.69 % of the three phases (calculated as oil comprising 40.7 % of the liquid phase, which constitutes 75.4 % of the total). Consequently, the percentage heights of the oil, gas, and water phases are determined to be 30.69 %, 24.60 %, and 44.71 %, respectively. Fig. 5e displays the experimentally measured and actual values of each phase holdup in the oil–gas-water three-phase flow, demonstrating errors of 0.55 %, 0.36 %, and 0.59 % in oil, gas, and water phases, respectively, thereby affirming the precision of the measurement method. The entire analytical procedure is explicated through the solution diagram depicted in Fig. 5f.

The experimental error primarily originates from measurement instruments (the errors caused by the data acquisition card, high voltage pulse generator, data cables and other equipment are included) and environmental noise, eventually reflected in the received signal. Therefore, uncertainty analysis on the transmitted signals under identical experimental conditions is conducted, as depicted in Figure S4. Ultimately, the calculated variance for the signal amounts to 0.027 (based on peak-to-peak value), indicating the stability of the measurement results. The comparison between the research presented in this paper and other studies is outlined as follows in Table 3.

Table 3
Comparison of the research results in this paper and those of other studies.

References	Measured parameters	Methods of measurement	Core devices	Research results and errors
Zhai et al. [49]	Oil holdup in horizontal oil–water two-phase flow pipes	Conductance method	Double helix capacitance sensor	The oil holdup ranging from 0 to 100 %, and the measurement error is 7.56 %
Han et al. [50]	Phase holdup in an airlift three-phase external circulation reactor	Resistance tomography combined with differential pressure method	ERT sensors and pressure sensors	The fluid holdup is about 60 %, and the error is less than 5 %
Sun et al. [51]	Gas-liquid two-phase carbon dioxide flow	Electrical capacitance tomography	Electrical capacitance tomography system and CO_2 two-phase flow rig	The gas holdup ranging from 0 to 77 %, and the absolute accuracy can reach 6 %
Xu et al. [52]	The water holdup of an oil–water two-phase flow in a horizontal oil well	Electrical conductance method	A dual-circle conductance probe array	The water holdup varies from 0 % to 100 %, and the RMSEs are 0.0632

5. Conclusion

In summary, this study presents a novel method for accurately measuring the holdup of three phases in small-size pipelines using an ultrasonic device featuring a flexible substrate, complemented by the introduction of the Specific Attenuation Coefficient (SAC) concept, resulting in holdup errors of less than 1 %. The self-manufactured ultrasonic device comprises two identical components, each incorporating a flexible substrate as a key element, striking a balance between the adaptability of the flexible probe and the durability of the rigid probe. An experimental and measurement system was established, facilitating multi-phase flow experiments utilizing the flexible ultrasound device. The verification of Reynolds numbers confirms laminar flow conditions within the experiment. Leveraging ultrasonic attenuation characteristics, SAC is introduced to differentiate between oil and water, enabling the quantification of three respective holdups by combining with transit-time principle. Ultimately, the measured phase holdups for oil, gas, and water are determined to be 30.69 %, 24.60 %, and 44.71 %, respectively. Since the initial set phase holdups of oil, gas and water are 30.87 %, 24.69 % and 44.44 %, respectively, thus, the error between the measured and actual values of oil, gas and water is 0.55 %, 0.36 % and 0.59 %, respectively, thereby affirming the accuracy of the measurement method. Furthermore, the variance of the measurement results is calculated to be 0.027, validating the stability of the measurement approach. This study effectively employs the ultrasonic device with a flexible substrate to assess the phase holdup of industrial three-phase flow, showcasing reliable outcomes, exhibiting strong adaptability, providing a straightforward theoretical framework, and employing cost-effective equipment, thus presenting numerous potential applications.

CRediT authorship contribution statement

Jinhui Fan: Writing – original draft, Methodology, Conceptualization. **Hang Liu:** Writing – original draft, Software, Methodology. **Haibin Cui:** Software. **Wenyuan Wang:** Formal analysis. **Jizhou Song:** Writing – review & editing, Writing – original draft. **Fei Wang:** Writing – review & editing, Funding acquisition.

Declaration of competing interest

The authors declare that they have no known competing financial interests or personal relationships that could have appeared to influence the work reported in this paper.

Data availability

No data was used for the research described in the article.

Acknowledgements

This work was supported by National Nature Science Foundation of China (No. 51976188).

Appendix A. Supplementary data

Supplementary data to this article can be found online at https://doi.org/10.1016/j.measurement.2024.114905.

References

[1] S.S. Kang, T.H. Kim, D.W. Cho, J.N. Kim, J.W. Kang, Continuous extraction of naphthenic acid from low-grade oil using 1,6-hexanediol in an ammonia solution, Fuel 332 (2023) 126008.
[2] N. Serio, M. Levine, Efficient extraction and detection of aromatic toxicants from crude oil and tar balls using multiple cyclodextrin derivatives, Mar. Pollut. Bull. 95 (1) (2015) 242–247.
[3] Z.J. Lu, J. Jiang, M.N. Ren, J.S. Xu, J.W. Da, F.H. Cao, The study on removing the salts in crude oil via ethylene glycol extraction, Energy Fuels 29 (1) (2015) 355–360.
[4] P.L. Spedding, G.F. Donnelly, E. Benard, Three-phase oil-water-gas horizontal co-current flow part II. Holdup measurement and prediction, Asia-Pac. J. Chem. Eng. 2 (2) (2007) 130–136.

[5] Y.J. Wang, J.L. Han, Z.Q. Hao, L.J. Zhou, X.J. Wang, M.W. Shao, A new method for measuring water holdup of oil-water two-phase flow in horizontal wells, Processes 10 (5) (2022) 848.
[6] G.Z. Fu, C. Tan, H. Wu, F. Dong, Adaptive Kalman estimation of phase holdup of water-continuous oil-water two-phase flow, IEEE Access 5 (2017) 3569–3579.
[7] Y. Wei, H.Q. Yu, Q. Chen, G.Q. Liu, C.X. Qi, J.F. Chen, A novel conical spiral transmission line sensor-array water holdup detection tool achieving full scale and low error measurement, Sensors 19 (19) (2019) 4140.
[8] Z. Gao, N. Jin, Nonlinear characterization of oil-gas-water three-phase flow in complex networks, Chem. Eng. Sci. 66 (12) (2011) 2660–2671.
[9] Z. Diermyer, Y. Xia, J. Li, Insights into waterflooding in hydrocarbon-bearing nanochannels of varying cross sections from mesoscopic multiphase flow simulations, Langmuir 39 (2023) 6992–7005.
[10] X. Cai, J. Li, X. Ouyang, Z. Zhao, M. Su, In-line measurement of pneumatically conveyed particles by a light transmission fluctuation method, Flow Meas. Instrum. 16 (5) (2005) 315–320.
[11] S. Zong, X. Zhang, S. Yang, Z. Duan, B. Chen, Laser backscattering characteristics of ship wake bubble target, CHIN OPT LETT 16 (6) (2023) 1333–1342.
[12] Y. Zheng, Q. Liu, Y. Li, N. Gindy, Investigation on concentration distribution and mass flow rate measurement for gravity chute conveyor by optical tomography system, Measurement 39 (7) (2006) 643–654.
[13] L.J. Xu, W. Zhang, Z. Cao, J.Y. Zhao, R.H. Xie, X.B. Liu, J.H. Hu, Water holdup measurement of oil-water two-phase flow in a horizontal well using a dual-circle conductance probe array, Meas. Sci. Technol. 27 (11) (2016) 77.
[14] D.J. McClements, Ultrasonic characterisation of emulsions and suspensions, Adv. Colloid Interface Sci. 37 (1991) 33–72.
[15] A.S. Dukhin, P.J. Goetz, Acoustic and electroacoustic spectroscopy, J. Am. Chem. Soc. 12 (1996) 4366.
[16] J. Fan, F. Wang, Ultrasonic simulation research of two-dimensional distribution in gas-solid two-phase flow by backscattering method, ARCH ACOUST 47 (3) (2022) 373–382.
[17] T. Xie, S.M. Ghiaasiaan, S. Karrila, T. Mcdonough, Flow regimes and gas holdup in paper pulp-water-gas three-phase slurry flow, Chem. Eng. Sci. 58 (8) (2003) 1417–1430.
[18] S. Wada, H. Kikura, M. Aritomi, M. Mori, Y. Takeda, Development of pulse ultrasonic doppler method for flow rate measurement in power plant multilines flow rate measurement on metal pipe, J. Nucl. Sci. Technol. 41 (3) (2004) 339–346.
[19] M. Takamoto, H. Ishikawa, K. Shimizu, H. Monji, G. Matsui, New measurement method for very low liquid flow rates using ultrasound, Flow Meas. Instrum. 12 (4) (2001) 267–273.
[20] C.H. Wang, X.S. Li, H.J. Hu, L. Zhang, Z.L. Huang, M.Y. Lin, Z.R. Zhang, Z.N. Yin, B. Huang, H. Gong, S. Bhaskaran, Y. Gu, M. Makihata, Y.X. Guo, Y.S. Lei, Y. M. Chen, C.F. Wang, Y. Li, T.J. Zhang, Z.Y. Chen, A.P. Pisano, L.F. Zhang, Q. F. Zhou, S. Xu, Monitoring of the central blood pressure waveform via a conformal ultrasonic device, Nat. Biomed. Eng. 2 (9) (2018) 687–695.
[21] W. Liu, C. Zhu, D. Wu, Flexible piezoelectric micro ultrasonic transducer array integrated on various flexible substrates, SENSOR ACTUAT A-PHYS 317 (2021) 112476.
[22] X.X. Ding, W. Li, J.T. Xiong, Y.F. Shen, W.B. Huang, A flexible laser ultrasound transducer for lamb wave-based structural health monitoring, Smart Mater. Struct. 29 (7) (2020) 075006.
[23] C. Peng, M. Chen, H.K. Sim, Y. Zhu, X. Jiang, Noninvasive and nonocclusive blood pressure monitoring via a flexible piezo-composite ultrasonic sensor, IEEE Sens. J. 21 (3) (2021) 2642–2650.
[24] T. La, L.H. Le, Flexible and wearable ultrasound device for medical applications: A review on materials, structural designs, and current challenges, Adv. Mater. Technol. 7 (3) (2021) 2100798.
[25] K. Meng, X. Xiao, W. Wei, G. Chen, A. Nashalian, S. Shen, X. Xiao, J. Chen, Wearable pressure sensors for pulse wave monitoring, Adv. Mater. 34 (21) (2022) 2109357.
[26] K.Y. Chun, S. Seo, C.S. Han, A wearable all-gel multimodal cutaneous sensor enabling simultaneous single-site monitoring of cardiac-related biophysical signals, Adv. Mater. 34 (16) (2022) 2110082.
[27] A.W. Guess, Calculation of perforated plate liner parameters from specified acoustic resistance and reactance, J. Sound Vib. 40 (1) (1975) 119–137.
[28] T. Alvarez-Arenas, Acoustic impedance matching of piezoelectric transducers to the air, IEEE Trans. Ultrason. Ferroelectr. Freq. Control 51 (5) (2004) 624–633.
[29] J.R. Allegra, S.A. Hawley, Attenuation of sound in suspensions and emulsions: Theory and experiments, J. Acoust. Soc. Am. 51 (5) (1971) 1545–1564.
[30] M. Su, M. Xue, X. Cai, Z. Shang, F. Xu, Particle size characterization by ultrasonic attenuation spectra, Particuology 6 (4) (2008) 276–281.
[31] B.J. Angelson, A theoretical study of the scattering of ultrasound from blood, IEEE Trans. Biomed. Eng. 27 (1980) 61–67.
[32] Q. Su, C. Tan, F. Dong, Mechanism modeling for phase fraction measurement with ultrasound attenuation in oil-water two-phase flow, Meas. Sci. Technol. 28 (3) (2017) 035304.
[33] D. Salvi, D. Boldor, J. Ortego, G.M. Aita, C.M. Sabliov, Numerical modeling of continuous flow microwave heating: A critical comparison of COMSOL and ANSYS, J. Microwave Power Electromagn. Energy 44 (4) (2010) 187–197.
[34] G.C. Liu, W.P. Cao, G.J. Zhang, Z.H. Wang, H.Y. Tan, J.W. Miao, Z.D. Li, W. D. Zhang, R.X. Wang, Design and simulation of flexible underwater acoustic sensor based on 3D buckling structure, Micromachines 12 (12) (2021) 1536.
[35] K. Tao, Z.S. Chen, J.H. Yu, H.Z. Zeng, J. Wu, Z.X. Wu, Q.Y. Jia, P. Li, Y.Q. Fu, H. L. Chang, W.Z. Yuan, Ultra-sensitive, deformable, and transparent triboelectric tactile sensor based on micro-pyramid patterned ionic hydrogel for interactive human-machine interfaces, Adv. Sci. Lett. 9 (10) (2022) 2104168.
[36] G. Huang, Q.H. Yang, Q. Xu, S.H. Yu, H.L. Jiang, Polydimethylsiloxane coating for a palladium/MOF composite: Highly improved catalytic performance by surface hydrophobization, Angew. Chem. Int. Ed. 55 (26) (2016) 7379–7383.
[37] S.A. Almatroodi, A. Almatroudi, A.A. Khan, F.A. Alhumaydhi, M.A. Alsahli, A. H. Rahmani, Potential therapeutic targets of epigallocatechin gallate (EGCG), themost abundant catechin in green tea, and its role in the therapy of various types of cancer, Molecules 25 (14) (2020) 3146.
[38] J. Hwang, Y. Kim, H. Yang, J.H. Oh, Fabrication of hierarchically porous structured PDMS composites and their application as a flexible capacitive pressure sensor, Compos. B 211 (2021) 108607.
[39] M.Q. Jian, K.L. Xia, Q. Wang, Z. Yin, H.M. Wang, C.Y. Wang, H.H. Xie, M.C. Zhang, Y.Y. Zhang, Flexible and highly sensitive pressure sensors based on bionic hierarchical structures, Adv. Funct. Mater. 27 (9) (2017) 1606066.
[40] T. Zhi, Y. Tafesse, B.M. Sadler, Cyclic feature detection with sub-Nyquist sampling for wideband spectrum sensing, IEEE J-STSP 6 (1) (2012) 58–69.
[41] F.P. Bretherton, The motion of rigid particles in a shear flow at low Reynolds number, J. Fluid Mech. 14 (02) (1962) 284–304.
[42] G.K. Batchelor, On steady laminar flow with closed streamlines at large Reynolds number, J. Fluid Mech. 1 (2) (2006) 177–190.
[43] S.F. Chekmarev, Laminar-turbulent transition: The change of the flow state temperature with the Reynolds number, J. Stat. Phys. 157 (6) (2014) 1019–1030.
[44] G.D. Zhang, X.B. Li, S.Z. Zhang, T. Kundu, Investigation of frequency-dependent attenuation coefficients for multiple solids using a reliable pulse-echo ultrasonic measurement technique, Measurement 177 (2021) 109270.
[45] M. Wang, D.D. Zheng, J. Dong, Y. Xu, Comparison of ultrasonic attenuation models for small droplets measurement based on numerical simulation and experiment, Appl. Acous 183 (2021) 108334.
[46] D. Liu, D.X. Niu, H. Wang, L.L. Fan, Short-term wind speed forecasting using wavelet transform and support vector machines optimized by genetic algorithm, Renew. Energy 62 (2014) 592–597.
[47] Y.H. Miao, M. Zhao, J. Lin, Y.G. Lei, Application of an improved maximum correlated kurtosis deconvolution method for fault diagnosis of rolling element bearings, Mech. Syst. Sig. Process. 92 (2017) 173–195.
[48] L. Zhai, N. Jin, Z. Gao, Z. Wang, Liquid holdup measurement with double helix capacitance sensor in horizontal oil-water two-phase flow pipes, Chin. J. Chem. Eng. 23 (1) (2015) 268–275.
[49] Y.H. Han, H. Jin, Experimental study on phase holdup in three-phase external loop airlift reactors using electrical resistance tomography, Chin. 9 (2009) 431–436.
[50] S. Sun W. Zhang S. J, Z. Cao, L. Xu, Y. Yan, Real-time imaging and holdup measurement of carbon dioxide under ccs conditions using electrical capacitance tomography IEEE Sens. J. 18 18 2018 7551 7559.
[51] L.J. Xu, W. Zhang, Z. Cao, J.Y. Zhao, R.H. Xie, X.B. Liu, J.H. Hu, Water holdup measurement of oil-water two-phase flow in a horizontal well using a dual-circle conductance probe array, Meas. Sci. Technol. 27 (11) (2016) 77.